G3, 2026, **16(1)**, jkaf260
https://doi.org/10.1093/g3journal/jkaf260
Advance Access Publication Date: 31 October 2025
Investigation

The C-terminal ZZ domain of the Drosophila ORB2 RNA-binding protein is required for spermatid individualization

Timothy C.H. Low,[1] Brook L. Falk ,[1,2] Julie A. Brill ,[1,2] Howard D. Lipshitz [1,*]

[1]Department of Molecular Genetics, University of Toronto, 661 University Avenue, Toronto Ontario M5G 1M1, Canada
[2]Program in Cell & Systems Biology, Research Institute, the Hospital for Sick Children, 686 Bay Street, Toronto, Ontario M5G 0A4, Canada

*Corresponding author: Department of Molecular Genetics, University of Toronto, 661 University Avenue, Toronto Ontario M5G 1M1, Canada.
Email: howard.lipshitz@utoronto.ca

ORB2 is the Drosophila ortholog of the human CPEB2-4 family of RNA-binding proteins, which include a conserved C-terminal Zinc-binding ('ZZ') domain. We have recently shown that this domain interacts with several translational co-repressors in the early embryo, and that deletion of this domain from the endogenous *orb2* gene results in derepression of its target mRNAs. Here we assess the effect of deletion of the ZZ domain on spermatogenesis. We find that deletion of the ZZ domain does not affect spatial localization of the ORB2 protein; $orb2^{\Delta ZZ}$ flies are sterile and lack mature sperm; meiosis is mostly normal in $orb2^{\Delta ZZ}$ testes; individualization complexes are defective and spermatid individualization fails; proteins known to play a role in spermatid individualization—ORB, IMP, SOTI—are mislocalized; and the SOTI-dependent Cleaved Caspase-3 gradient no longer forms in $orb2^{\Delta ZZ}$ mutant testes.

Keywords: ORB2; cytoplasmic polyadenylation element binding protein (CPEB); RNA-binding protein (RBP); post-transcriptional regulation; spermatogenesis; meiosis; SOTI; cleaved caspase 3 (CC3); IMP; ORB

Introduction

Proteins belonging to the cytoplasmic polyadenylation element binding (CPEB) family are highly conserved RNA-binding proteins that canonically interact with U-rich cytoplasmic polyadenylation element (CPE) motifs found in the 3′UTR of target transcripts (Hake and Richter 1994; Ivshina et al. 2014). Most animals, including humans, mice, and *Caenorhabditis elegans*, have four CPEB genes (where CPEB2-4 are more closely related to each other than to CPEB1), whereas *Drosophila* has two: *orb* and *orb2*. While the N-terminal portion of CPEB proteins is divergent, there are high levels of homology at the C-terminus of CPEB proteins, mostly concentrated at the tandem RNA-recognition motifs (RRMs) that serve as the RNA-binding domain (RBD) and the adjacent ZZ-class zinc binding domain.

The defining feature of ZZ domains is coordination of two Zn^{2+} ions, which is accomplished in dystrophin and in CREB-binding protein by Cys-X_2-Cys motifs, and in the CPEB protein family by six cysteine and two histidine residues (Ponting et al. 1996; Legge et al. 2004; Merkel et al. 2013). NMR structural analysis of CPEB1's ZZ domain shows that it folds into a cross-braced zinc ligand topology, in which a β hairpin and an α helix are brought together; this structure is homologous to that of known RING and PHD motifs (Merkel et al. 2013). In general, ZZ domains are known to facilitate protein-protein interactions. For example, the ZZ domain of HERC2 recognizes arginylated protein substrates (Tencer et al. 2022), the ZZ domain of *Schizosaccharomyces pombe* Nbr1 recognizes distinct protein cargos (Wang et al. 2021), several reports have shown that the ZZ domains of CPB and HERC2 are able to recognize SUMOylated substrates (Danielsen et al. 2012; Diehl et al. 2016; Park et al. 2017; Liu et al. 2020), and we have recently reported that the ZZ domain of Drosophila ORB2 interacts with the Cup translational repressor complex and the 43S Preinitiation Complex (PIC) in early embryos (Low et al. 2025).

CPEB2-4 and their homologs are expressed in both soma and the germline, with functions in the nervous system, asymmetric stem cell division, and gametogenesis (Ivshina et al. 2014). In *Drosophila*, *orb2* is enriched in the testis, where it is essential for many stages of spermatogenesis (Xu et al. 2012; Vedelek et al. 2018; Li et al. 2022). The *orb2* locus produces two protein isoforms, and both are expressed in the testis; the 60-kDa ORB2A and the 75-kDa ORB2B isoforms share 542 amino acids consisting (N-to-C) of a poly-glutamine (polyQ) tract, a predicted intrinsically disordered region (IDR), the RBD, and the ZZ domain; they differ only at their N-termini, which contain 9 and 162 unique amino acid sequences, respectively.

In the testis (diagramed in Fig. 1), ORB2 is detectable after the completion of mitosis in the 16-cell cysts, where expression of both *orb2* mRNA and protein rapidly increase and peak during and after meiosis, specifically at the 32- and 64-cell secondary spermatocyte and spermatid cysts (Xu et al. 2012). Subsequently, ORB2 persists and is distributed along the entire spermatid bundle, with the highest concentration found at the distal end of the

Received on 18 August 2025; accepted on 25 October 2025
© The Author(s) 2025. Published by Oxford University Press on behalf of The Genetics Society of America.
This is an Open Access article distributed under the terms of the Creative Commons Attribution License (https://creativecommons.org/licenses/by/4.0/), which permits unrestricted reuse, distribution, and reproduction in any medium, provided the original work is properly cited.

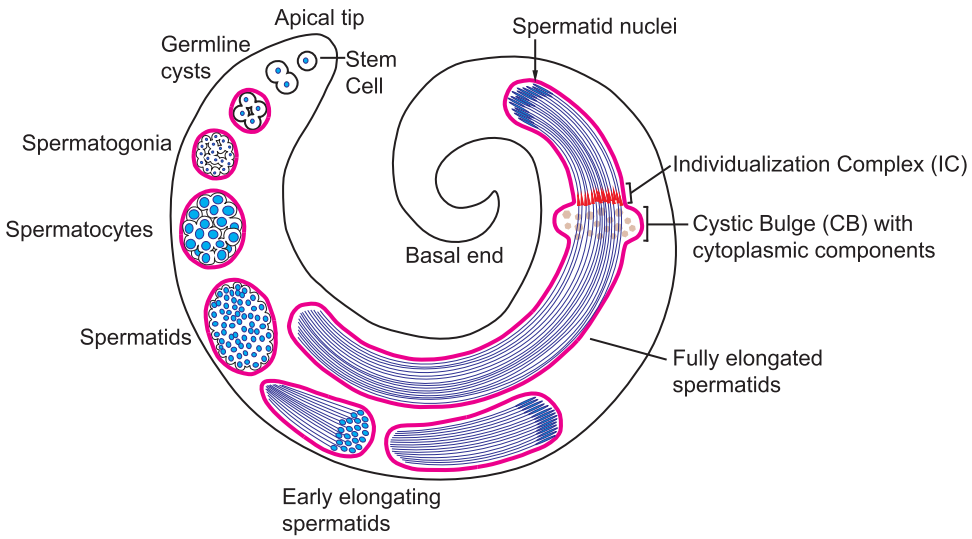

Fig. 1. Diagram depicting the stages of spermatogenesis as they are spatiotemporally organized in the Drosophila testis. Germline cysts (outlined in magenta) are oriented with spermatid nuclei pointing toward the basal end and sperm tails pointing toward the apical tip. Cysts travel from the apical tip toward the basal end as they mature. Nuclei are colored blue.

growing flagellar axonemes. This expression pattern corresponds with the phenotype of *orb2* null mutants, in which spermatocytes fail to complete meiosis and have defects in spermatid differentiation; these disruptions cause male sterility (Xu et al. 2012, 2014). In addition, deletion of the *orb2* mRNA's 3'UTR has no effect on meiosis, but results in defects in spermatid individualization that may be attributable to mislocalization of *orb2* mRNA and ORB2 protein in the 64-cell cyst (Gilmutdinov et al. 2021).

We recently reported that, in early embryos, ORB2 protein interacts with hundreds of target transcripts and physically interacts with multiple translational repressors (Low et al. 2025). We generated an endogenous deletion of the ZZ domain ($orb2^{\Delta ZZ}$) produced by CRISPR, which retains the endogenous RBD and 3'UTR, binds to target RNAs but loses interaction with many of the co-repressors, resulting in derepression of target mRNA translation during the maternal-to-zygotic transition (Low et al. 2025). $orb2^{\Delta ZZ}$ females are fertile and their embryos have no overt developmental phenotypes (Low et al. 2025).

Here, we show that male $orb2^{\Delta ZZ}$ flies are sterile and we assess the role of the ZZ domain during spermatogenesis in the adult testis. We show that the ZZ domain has a minor role during meiosis but is essential for spermatid individualization, failure of which leads to male sterility in $orb2^{\Delta ZZ}$ mutants. Loss of the ZZ domain results in increased levels of ORB2 but does not affect its spatial expression in the testis. In $orb2^{\Delta ZZ}$ mutant testes, individualization complexes (ICs) are mispositioned and actin cones are scattered. Moreover, ORB, IMP, SOTI and Cleaved caspase-3 (CC3) are mislocalized. Our data are consistent with a model in which the ZZ domain of ORB2 is required for organization of the distal region of the spermatid cyst and establishment of the SOTI gradient, which in turn regulates CC3 production and successful spermatid individualization.

Materials and methods

Fly stocks

The following *Drosophila melanogaster* stocks were used: w^{1118} is the host, pre-injected w^{1118} line that was used to generate the CRISPR $orb2^{\Delta ZZ}$ mutant line (Low et al. 2025). Mutants analyzed were $orb2^{\Delta ZZ}$ (Low et al. 2025), $orb2^{36}$ and $orb2^{7}$ (Xu et al. 2012). Adult $orb2^{\Delta ZZ}/orb2^{36}$ and $orb2^{\Delta ZZ}/orb2^{7}$ flies were obtained by crossing homozygous $orb2^{\Delta ZZ}$ virgin females with $orb2^{36}$/balancer or $orb2^{7}$/balancer males. The methods used to generate $orb2^{\Delta ZZ}$ are described in (Low et al. 2025); orb^{36} (BDSC#58479, RRID: BDSC_58479) and $orb2^{7}$ (BDSC#58480; RRID:BDSC_58480) were obtained from the Bloomington Drosophila Stock Center, deposited by Paul Schedl. Details of the stocks can be found on FlyBase (Ozturk-Colak et al. 2024). Flies were cultivated at 25 °C under standard laboratory conditions unless otherwise indicated.

RT-qPCR

RNA was isolated from 1- to 3-d post-eclosion adult testes using TRI Reagent (Sigma) according to manufacturer's instructions. Isolated RNA was quantitatively reverse transcribed into single-stranded cDNA with the Superscript IV reverse transcriptase kit (Invitrogen) according to manufacturer's instructions. 500 ng of total RNA per sample was used to synthesize cDNA, which was primed using random hexamer primers. The resulting single-stranded cDNA was diluted 1:25 using RNase-free water and used to perform quantitative real-time PCR with primers specific to various transcripts assayed as derived from FlyBase (Supplementary Fig. 1) (Ozturk-Colak et al. 2024). Primers specific to the transcripts assayed were designed using NCBI Primer-BLAST. Quantitative real-time PCR was performed with SensiFAST SYBR PCR mix (Bioline) following the manufacturer's protocol and using 5 µL of diluted cDNA per reaction. A CFX384 Real-Time System (Bio-Rad) was used to carry out the PCR reaction.

The results of the qPCR were analyzed using CFX Manager software (Bio-Rad). Each biological replicate represents a measurement obtained for a separate set of testis dissections; values from three technical replicates were averaged and relative gene expression was normalized to the transcripts *RpL32* and *GAPDH2* as normalization controls. Normalized expression is presented as the average of three biological replicates with error bars representing standard deviation; P-values were calculated by one-way ANOVA.

Antibodies

The following primary antibodies were used: mouse anti-ORB2 4G8 (1:50 for Western blot, 1:200 for immunostaining; obtained from the Developmental Studies Hybridoma Bank), mouse anti-ORB 6H4 (1:200 for immunostaining; obtained from the Developmental Studies Hybridoma Bank), rabbit anti-IMP (1:100 for immunostaining; gifted by Paul Macdonald), Guinea pig anti-SOTI (1:50 for immunostaining; gifted by Eli Arama), rabbit monoclonal anti-Cleaved Caspase 3 (Asp175, Cell Signaling Technology). Mouse anti-Actin (Sigma) was used at 1:10,000 for Western blots as a loading control. The following secondary antibodies were used in the immunostaining: goat anti-mouse Alexa555, goat anti-mouse Alexa488, goat anti-rabbit Alexa555, goat anti-rabbit Alexa488, and donkey anti-Guinea pig Cy3.

Western blots

Proteins were resolved by SDS-PAGE and transferred to PVDF membrane, blocked at room temperature for 30 min with 1% non-fat milk in PBST (1xPBS supplemented with 0.1% Tween20). Blots were hybridized with primary antibodies in 1% non-fat milk in PBST at 4 °C overnight while nutating. HRP-conjugated secondary antibodies were hybridized to the blot at 1:5,000 dilution in 1% non-fat milk in PBST at 20 °C while nutating for 1 h. Blots were developed using ECl detection substrate (Millipore Immobilon Luminata Crescendo Western HRP substrate) and imaged with ChemiDoc and ImageLab (BioRad).

Blot band intensities were quantified using ImageLab. The Lane and Bands tool was used to annotate the lanes, and the Detect Bands tool and Analyze Bands functions were used to determine band intensities. ImageLab automatically subtracts background noise from the band intensities. Since we included a dilution series on the blot, the highest intensity band was selected as the Reference band, and lane input quantities (100%, 50%, and 25%) were annotated. Volumetric band intensities of all bands of interest were normalized to the band intensity of the Actin band in each corresponding lane. For each genotype, the calculated band intensity (normalized to Actin) was averaged across all three input quantities to obtain the final amount for that genotype. Finally, the band intensity for mutant proteins was normalized to the band intensity for w^{1118} proteins to obtain relative expression levels.

Male fertility assay

Individual male flies were crossed with two or three w^{1118} virgin females in a vial with yeast pellets for seven days; the adults were removed, and the vials were scored for the presence of larvae, pupae, and adults for the following seven days. Males whose matings produced larvae were scored as fertile.

Testis immunostaining

For whole mount α-ORB2, α-IMP, α-ORB, and α-SOTI staining (Figs. 2 and 6–8), testes from 1- to 3-day old flies were dissected in 4 °C PBS and fixed with 1% paraformaldehyde for 20 min. After fixation, testes were washed three times with PBST (1 × PBS + 0.1% Tween-20) for 5 min (here and below). Testes were then washed twice with PBST and incubated with a solution of 0.1% Tween-20 and 0.3% Triton X-100 in 1 × PBS) with 5% normal goat serum (Life Technologies) at room temperature for 1 h, which was followed by an overnight incubation with primary antibody and/or rhodamine phalloidin. This was followed by three washes with PBST and incubation with secondary antibody for 2 h. After three final washes with PBST, testes were mounted on slides with DAPI in DABCO mounting media. Images were acquired on an inverted Leica DMi8 epifluorescence microscope with a 40× phase-contrast objective and Leica K5 camera using the Thunder Imaging System.

For Hoechst staining (Fig. 4), testes were dissected in cold PBS with Hoechst-33342 (1:1,000) and transferred onto poly-L-lysine coated slides with a drop of PBS and Hoechst (as above). The apical tip of each testis was cut off, a coverslip was placed on top, and excess PBS was removed with a Kimwipe to draw cells out of the testis sheath. Images were acquired on an inverted Leica DMi8 epifluorescence microscope with a 40× phase-contrast objective and Leica K5 camera using the Thunder Imaging System. Images were uniformly processed for brightness and contrast using LAS-X software.

For α-CC3 (Fig. 9), 1- to 3-day old testes were dissected in testis isolation buffer (183 mM KCl, 47 mM NaCl, 10 mM Tris pH 6.8) and transferred onto a poly-L-lysine coated slide. Coverslips were placed over the testes, which were flattened by drawing off liquid with a Kimwipe. Slides were frozen in liquid nitrogen for 10 s before the coverslip was removed with a razor blade. Slides were incubated in −20 °C 95% ethanol for 10 min. Samples were fixed in 4% paraformaldehyde for 7 min, washed in PBS + 0.1% Triton X-100, permeabilized in PBS + 0.3% Triton X-100 + 0.3% Na Deoxycholate for 15 min twice, washed for 10 min, and blocked in PBS + 0.1% Triton X-100 + 5% Bovine Serum Albumin for 30 min. Samples were incubated overnight in blocking solution with α-CC3 (1:400), washed thrice for 5 min and once for 15 min, and incubated with secondary antibody for one hour. Samples were washed for 15 min, incubated for 15 min in PBS + 0.1% Triton X-100 with DAPI (1:1000) and 30 min in PBS + 0.1% Triton X-100 with rhodamine-phalloidin (1:200). Following this, samples were washed twice for 15 min and mounted using fluorescence mounting medium. Images were acquired on an inverted Nikon A1R laser scanning confocal with 10× and 60× objectives using NIS Elements software. Images were uniformly processed for brightness and contrast using Volocity software. Experimental replicates were carried out with the following modifications: testes were dissected in cold PBS and transferred into membrane-lined trays in four-well plates where they were fixed for 30 min, permeabilized for 30 min in PBS + 0.3% Triton X-100, blocked in PBS + 0.3% Triton X-100 + 0.5% BSA, and mounted onto poly-L-lysine coated slides in Vectashield Antifade Mounting Medium with DAPI. Similar phenotypes were observed with both protocols.

Results

Deletion of the ZZ domain results in increased expression of orb2 mRNA and ORB2 protein in testes

To determine whether deletion of the ZZ domain affects expression of the *orb2* gene in testes, we examined levels of transcripts in testis extracts by RT-qPCR and protein by Western blot (Fig. 2). RT-qPCR of *orb2* mRNA in testis extracts showed that $orb2^{\Delta ZZ}$ transcripts were present at roughly double the level in $orb2^{\Delta ZZ}$ homozygous testes compared to WT *orb2* transcripts in w^{1118} testes (Fig. 2a and Supplementary Fig. S1). $orb2^{\Delta ZZ}$ mRNA levels were comparable to *orb2* levels in wild type when $orb2^{\Delta ZZ}$ was present in a single copy in combination with either of two previously reported *orb2* deletion mutants—$orb2^{36}$ and $orb2^{7}$—which each harbor a different targeted deletion of the *orb2* locus (Fig. 2a) (Xu et al. 2012). To ensure that the $orb2^{\Delta ZZ}$ transcripts contained the precise ZZ domain deletion, we also used a pair of primers that span the deletion site to quantify the levels of $orb2^{\Delta ZZ}$ transcript in testis extract from each genotype (Supplementary Fig. 1). As expected, no PCR

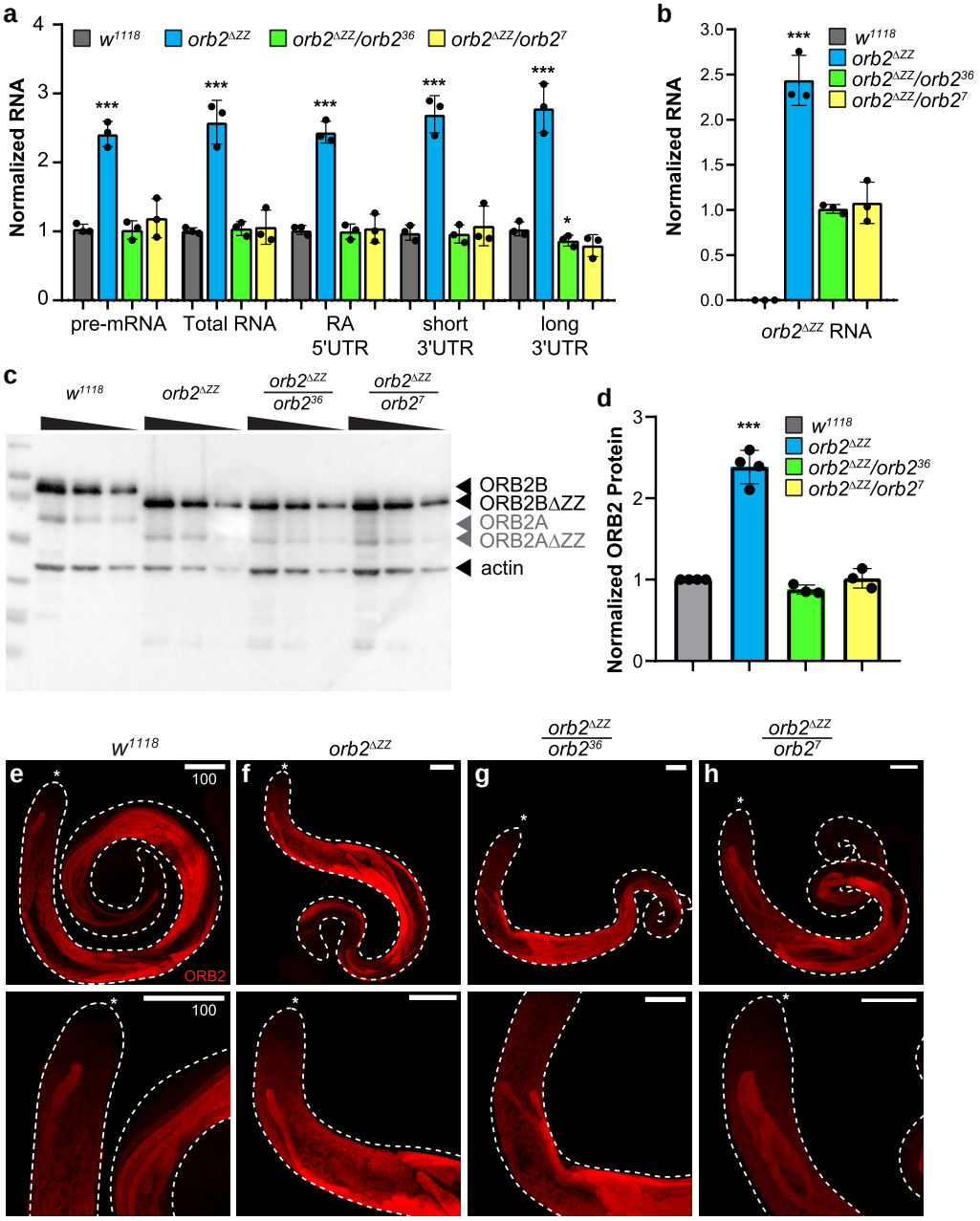

Fig. 2. Expression of *orb2* mRNA and ORB2 protein in testes. a) and b) Bar graphs showing the expression of various *orb2* mRNA isoforms (primer targets shown on the x-axis and diagramed in Supplementary Fig. 1) measured by RT-qPCR from testis extract prepared from four different genotypes (indicated by bar color). RNA levels shown are double normalized, first to *RpL32* and *GAPDH2* mRNAs, and then to w^{1118}. c) Western blot showing the expression of ORB2 and ORB2ΔZZ protein in testis extracts. d) Bar graph showing the quantification of ORB2 and ORB2ΔZZ protein levels normalized to Actin loading control; $n = 4$. e to h) Confocal microscopy images of testes stained for ORB2 in the genotypes indicated. Asterisk (*) marks the apical tip of the testis; scale bars represent 100μm.

amplification of $orb2^{\Delta ZZ}$ transcript was detected in w^{1118} testes (Fig. 2b), while expression levels in the $orb2^{\Delta ZZ}$ homozygote and $orb2^{\Delta ZZ}$/deletion (either $orb2^{36}$ or $orb2^{7}$) hemizygotes were comparable to that shown in Fig. 2a.

We next examined protein expression and found that, consistent with our analyses of mRNA, there was two-fold more ORB2ΔZZ protein in $orb2^{\Delta ZZ}$ testes than ORB2 protein in wild-type testes (Fig. 2, c and d). Also consistent with the mRNA results, ORB2ΔZZ protein levels in testes from $orb2^{\Delta ZZ}$/deletion heterozygous flies were comparable to ORB2 protein levels in wild-type testes (Fig. 2, c and d).

Over-expression of $orb2^{\Delta ZZ}$ mRNA and ORB2ΔZZ protein is likely due to loss of negative autoregulation, since ORB2 is known to regulate expression of its own mRNA (Mastushita-Sakai et al. 2010; Stepien et al. 2016; Low et al. 2025).

Deletion of the ZZ domain does not affect spatial expression of ORB2 in testes

To determine whether the expression pattern and localization of ORB2 protein in the testis is affected by the ZZ domain deletion, we stained 3-day old testes with mouse anti-ORB2 antibodies and examined the expression of ORB2 protein by laser scanning

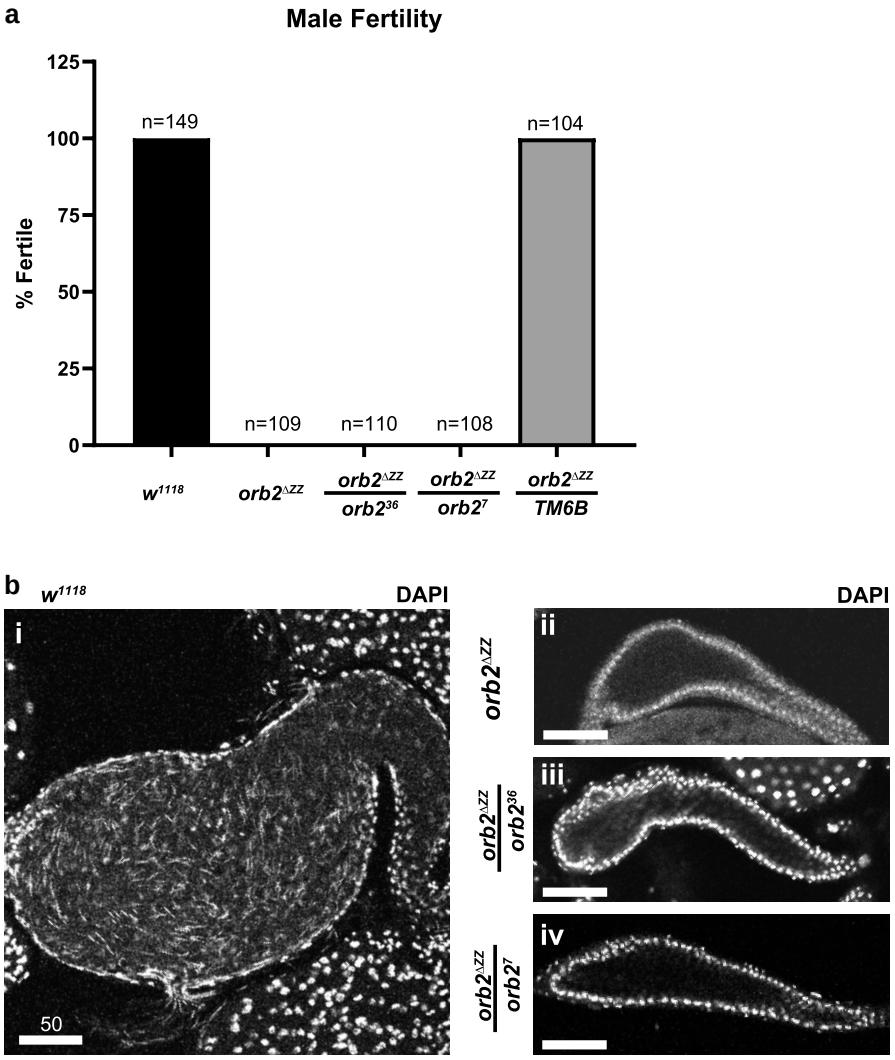

Fig. 3. *orb2*$^{\Delta ZZ}$ males are sterile and have empty seminal vesicles. a) Bar graph showing the results of the male fertility assay, presented as a percentage. b) Laser-scanning confocal micrographs of whole seminal vesicles stained with DAPI (white). In w^{1118} testes, the seminal vesicle is large and full of mature sperm, which can be identified by the needle-shaped nuclei; the seminal vesicle of *orb2*$^{\Delta ZZ}$ flies is empty and lacks mature sperm. Scale bars represent 50 μm.

confocal microscopy (Fig. 2, e to h). Consistent with previous reports (Xu et al. 2012; Gilmutdinov et al. 2021), in w^{1118} testes there was little to no ORB2 protein in the stem cells and low levels began to be detected in early primary spermatocytes (Fig. 2e). After completion of mitosis, as the spermatogonia transitioned through S-phase into primary spermatocytes, there was a significant increase in ORB2 protein corresponding with the extended G2 phase associated with high levels of transcription and stockpiling of gene products required for subsequent processes. ORB2 protein persisted in the post-meiotic 64-cell cysts as they underwent the process of spermatid elongation, where it was distributed along the entire length of the sperm tails, with a slight enrichment of ORB2 protein in the distal end of elongated spermatid cysts (i.e. the opposite end to the nuclei) (Fig. 2e).

In the *orb2*$^{\Delta ZZ}$ homozygous mutant testes, while the level of ORB2ΔZZ was increased as described (Fig. 2, c and d), the spatial expression pattern was indistinguishable from w^{1118} testes (Fig. 2f). We also examined the expression of ORB2ΔZZ protein in testes dissected from *orb2*$^{\Delta ZZ}$/deletion heterozygotes and, again, found that the expression pattern of ORB2ΔZZ protein was comparable to that in w^{1118} testes (Fig. 1, g and h).

Taken together, these results indicate that the timing and expression pattern of the ORB2ΔZZ protein is similar to that of wild-type ORB2 protein during spermatogenesis.

orb2$^{\Delta ZZ}$ males are sterile and do not produce mature sperm

Complete deletion of the *orb2* gene (Xu et al. 2012) causes 100% male sterility while deletion of only its 3′UTR causes sterility in ~80% of males examined (Gilmutdinov et al. 2021). To determine whether deletion of the ZZ domain has any effect on male fertility, we performed a fertility assay on adult male *orb2*$^{\Delta ZZ}$ mutant flies, where single males were paired with two or three virgin w^{1118} females, and fertility was scored by the presence or absence of larvae in the vial after seven days. *orb2*$^{\Delta ZZ}$ mutants were completely sterile both as *orb2*$^{\Delta ZZ}$ homozygotes and when heterozygous with *orb2* deletion alleles (Fig. 3a). To assess whether mature sperm were produced, we examined DAPI-stained seminal vesicles. Wild-type seminal vesicles from w^{1118} males were large and full of mature sperm, as indicated by the needle-shaped nuclei of the mature sperm (Fig. 3b). For all three *orb2*$^{\Delta ZZ}$ mutant genotypes,

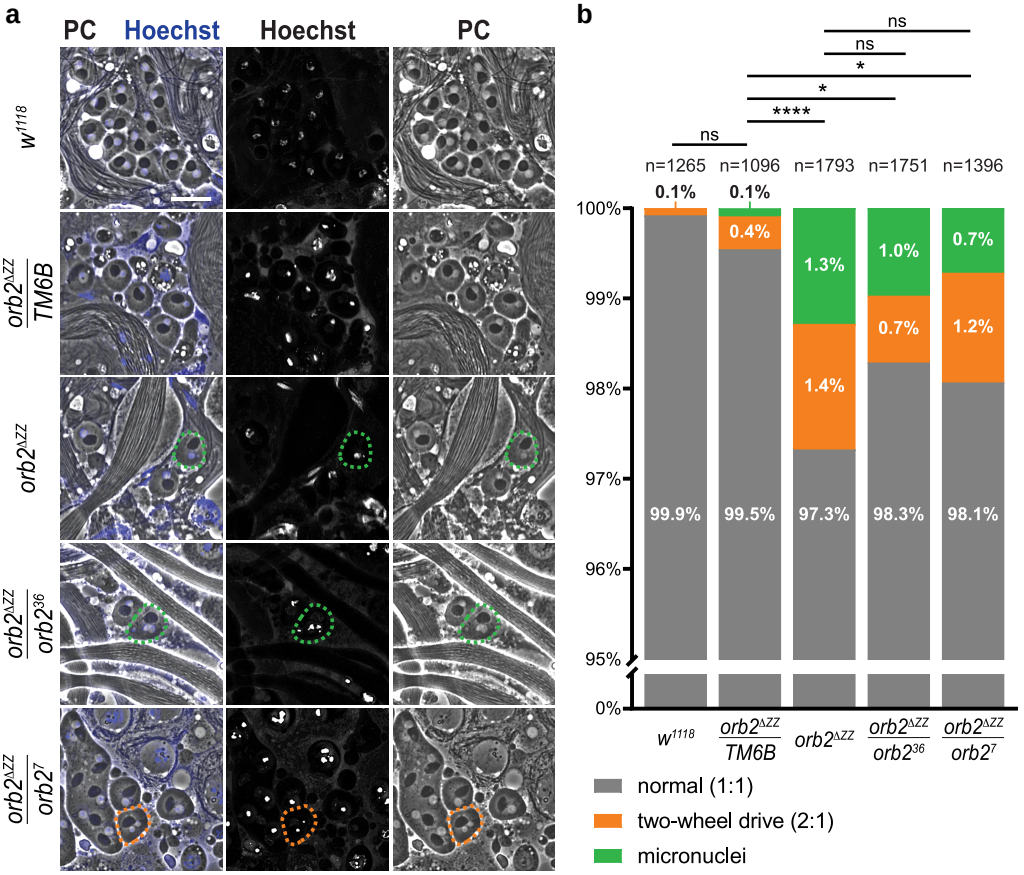

Fig. 4. *orb2*$^{\Delta ZZ}$ males show mild defects in meiosis. a) Phase contrast (PC) and epifluorescence micrographs with Hoechst staining (blue) of squashed adult testes. Orange cell outline identifies a post-meiotic spermatid with a 2:1 nucleus to Nebenkern ratio (also called a "two-wheel drive" phenotype); green cell outline identifies a post-meiotic spermatid with micronuclei. Scale bar represents 20 μm. b) Bar graph depicting the frequency of abnormal nucleus to Nebenkern ratios in post-meiotic spermatids. Gray represents the percentage of post-meiotic spermatids with a 1:1 nucleus to Nebenkern ratio; orange represents percentage with a 2:1 nucleus to Nebenkern ratio; green represents percentage with micronuclei. *n* indicates the number of post-meiotic round spermatids examined. Fisher's exact test with Bonferroni correction for multiple comparisons; ns, not significant, $P > 0.05$; *$P \leq 0.05$; ****$P \leq 0.0001$.

the seminal vesicles were small and empty, as indicated by the lack of sperm heads (Fig. 3b).

Meiosis is mostly normal in orb2$^{\Delta ZZ}$ homozygous males

Successful completion of meiosis results in 64 spermatids which have a light nucleus in phase contrast microscopy (also identifiable by positive Hoechst staining) that is paired with a dark mitochondrial Nebenkern. Spermatocytes in *orb2*^{36} mutants do not complete meiosis, the Nebenkern is poorly contrasted and, occasionally, fragmented (Xu et al. 2012).

To assess defects in meiosis upon loss of the ZZ domain, we produced and examined testis squashes (using phase contrast microscopy and staining with Hoechst) from five different genotypes: the pre-injected *w*^{1118} host strain that was used for CRISPR, heterozygous *orb2*$^{\Delta ZZ}$/TM6B (which contains a single copy of the ZZ deletion allele and a single wild-type copy of *orb2*), homozygous *orb2*$^{\Delta ZZ}$, and the two hemizygous genotypes—*orb2*$^{\Delta ZZ}$/*orb2*^{36} and *orb2*$^{\Delta ZZ}$/*orb2*^{7}—that each contain one copy of the *orb2*$^{\Delta ZZ}$ allele paired with one of the two *orb2* deletion alleles (Fig. 4). 99.9 and 99.5% of post-meiotic spermatids in the *w*^{1118} and *orb2*$^{\Delta ZZ}$/TM6B heterozygous controls, respectively, exhibited a nucleus-to-Nebenkern ratio of 1:1. In *orb2*$^{\Delta ZZ}$ homozygotes 2.7% of the spermatids either had a 2:1 ratio of nuclei to Nebenkern (also known as a "two-wheel drive" phenotype) or several micronuclei instead of a single nucleus. In the two hemizyous genotypes, these defects accounted for 1.7 and 1.9% of nuclei in *orb2*$^{\Delta ZZ}$/*orb2*^{36} and *orb2*$^{\Delta ZZ}$/*orb2*^{7}, respectively.

Spermatid individualization fails in orb2$^{\Delta ZZ}$ mutants

We next assessed whether *orb2*$^{\Delta ZZ}$ mutants exhibited defects later in spermatogenesis, notably during spermatocyte individualization, a process defective in null *orb2* mutants (Xu et al. 2012, 2014). We stained for actin and DNA in 3-day old testes to examine the nuclear bundles and individualization complexes (IC, which contain investment cones that are marked by F-actin) formation and progression (diagramed in Fig. 1). In wild-type testes, the spermatid nuclei condense and assemble into tight bundles during elongation (Fig. 5ai'). Once elongation is complete, the process of individualization begins with investment cones rich in filamentous actin that gather around each needle-shaped nucleus (Fig. 5ai"). The actin cones bundle together to form the IC and travel synchronously away from the nuclei (Fig. 5aii), a process that ensheathes each flagellar axoneme with its own plasma membrane and pushes the excess cytoplasm into a cystic bulge (CB) (Fig. 5aiii).

In *orb2*$^{\Delta ZZ}$ homozygous, *orb2*$^{\Delta ZZ}$/*orb2*^{36}, and *orb2*$^{\Delta ZZ}$/*orb2*^{7} testes, multiple nuclei were present outside of bundles and fragmenting

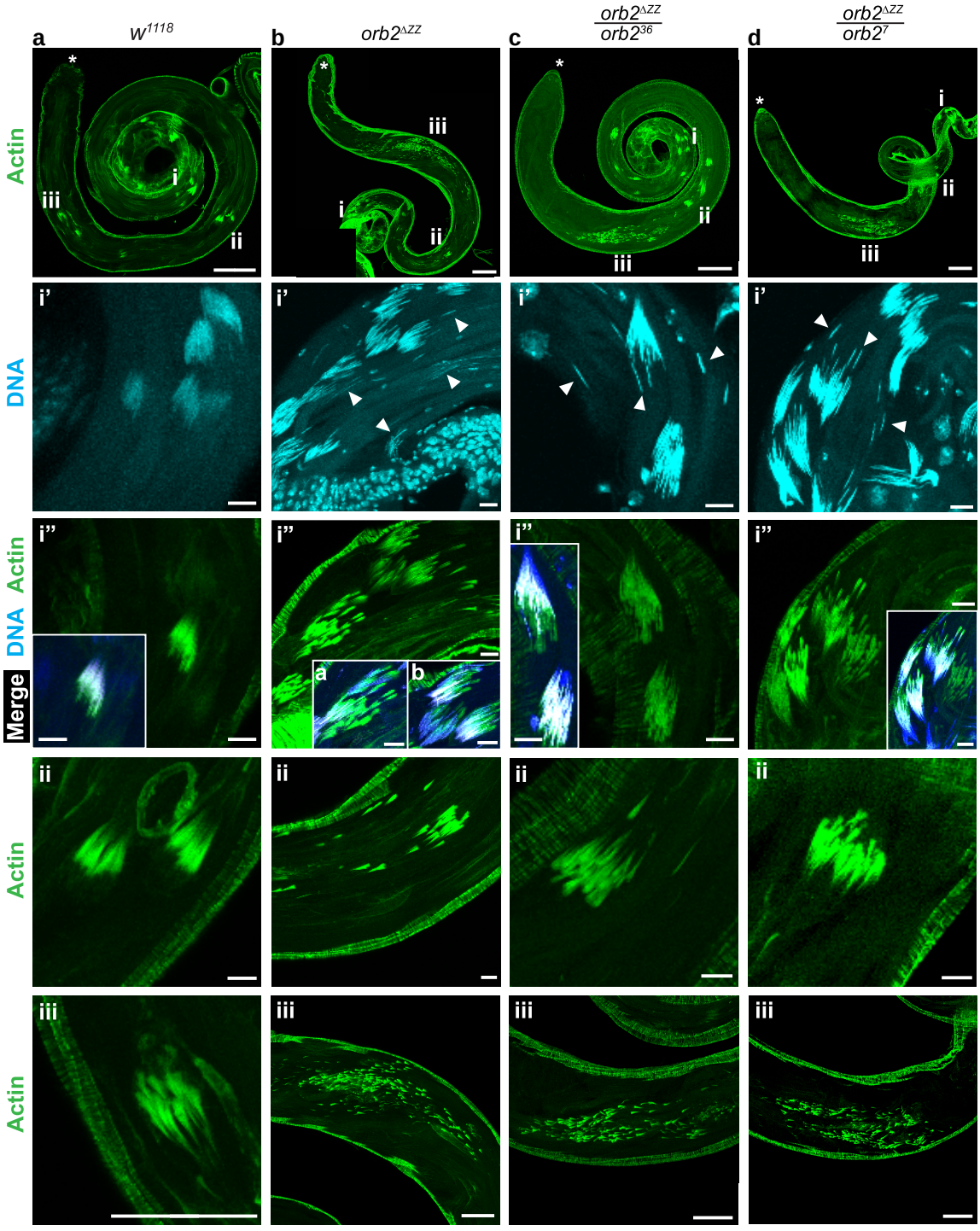

Fig. 5. Actin cones in the individualization complex are scattered in $orb2^{4ZZ}$ testes. Laser-scanning confocal micrographs of whole adult testes stained for F-actin with phalloidin-FITC (green) and for DNA with DAPI (blue) showing the organization of actin cones in four genotypes. a) w^{1118}; b) $orb2^{4ZZ}$; c) $orb2^{4ZZ}/orb2^{36}$ testis. d) $orb2^{4ZZ}/orb2^{7}$ testis. Asterisk (*) indicates the apical tip of testis; scale bars represent 50 μm for the top row of panels. Region i shows early individualization, scale bars represent 10 μm: panel i' shows DNA staining of nuclei organized into nuclear bundles, and arrowheads indicate scattered/non-bundled nuclei; panel i" shows actin staining of individualization cones forming around each nucleus, inset shows merged image of i' and i", where blue is DNA, green is Actin, and white is the overlap; scale bars represent 10 μm. Region ii depicts ICs for cysts mid-individualization; in w^{1118}, $orb2^{4ZZ}/orb2^{36}$, and $orb2^{4ZZ}/orb2^{7}$, these ICs appear mostly intact, but $orb2^{4ZZ}$ ICs are already dissociating and becoming scattered; scale bars represent 10 μm. Region iii depicts ICs for cysts in late individualization; all three mutant genotypes have extremely scattered actin cones at this stage; scale bar in aiii represents 10 μm, and scale bars in biii-Diii represent 50 μm. The images shown are representative of 100% of testes examined: w^{1118} ($n = 43$); $orb2^{4ZZ}$ ($n = 36$); $orb2^{4ZZ}/orb2^{36}$ ($n = 24$); $orb2^{4ZZ}/orb2^{7}$ ($n = 23$).

bundles could also be observed (Fig. 5, b to d, panels i'). At the early stages of individualization, actin cones assembled around each nucleus in wild type (Fig. 5a, panel ii). However, in the mutants, as the ICs migrated away from the sperm head, actin cones became extremely scattered (Fig. 5, b to d panels ii and iii), and none of the ICs remained intact in any of the testes examined

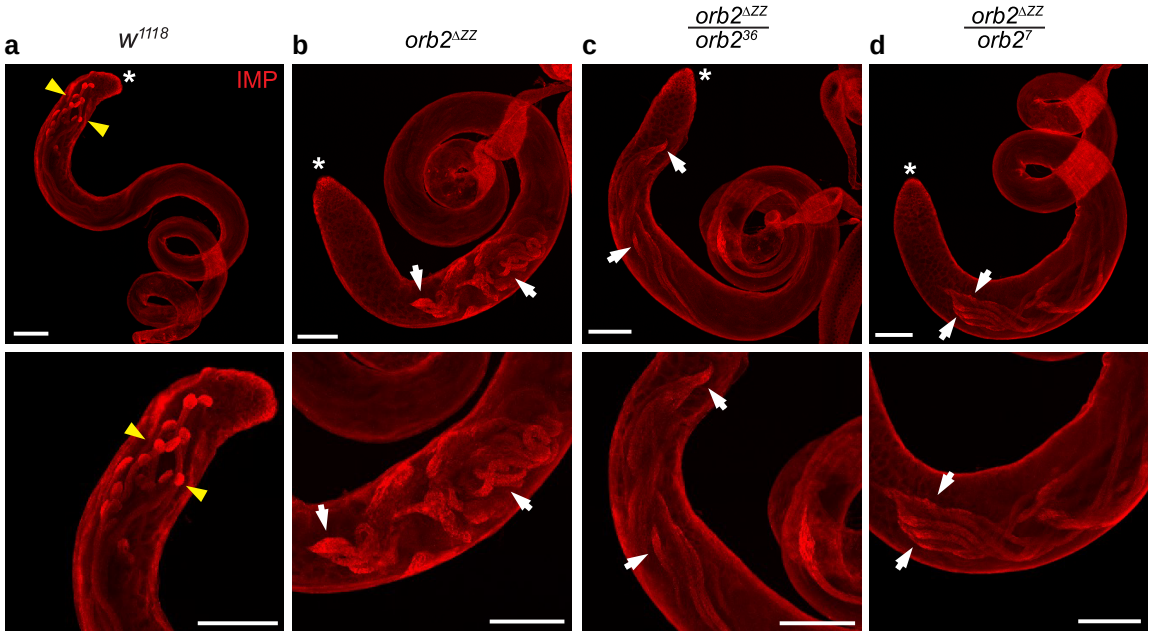

Fig. 6. Spatial distribution of IMP protein is disrupted in $orb2^{\Delta ZZ}$ testes. Laser-scanning confocal micrographs of whole adult testes stained for IMP. a) w^{1118}; b) $orb2^{\Delta ZZ}$; c) $orb2^{\Delta ZZ}/orb2^{36}$; d) $orb2^{\Delta ZZ}/orb2^{7}$. Asterisk (*) indicates the apical tip of the testis; scale bars represent 100 μm; arrowheads in (a) indicate localized IMP protein, concentrated at the distal ends of cysts of elongating spermatids; arrows in (b) to (d) indicate abnormal localization and/or expression patterns in mutant testes. The images shown are representative of 100% of testes examined: w^{1118} ($n = 14$); $orb2^{\Delta ZZ}$ ($n = 11$); $orb2^{\Delta ZZ}/orb2^{36}$ ($n = 12$); $orb2^{\Delta ZZ}/orb2^{7}$ ($n = 12$).

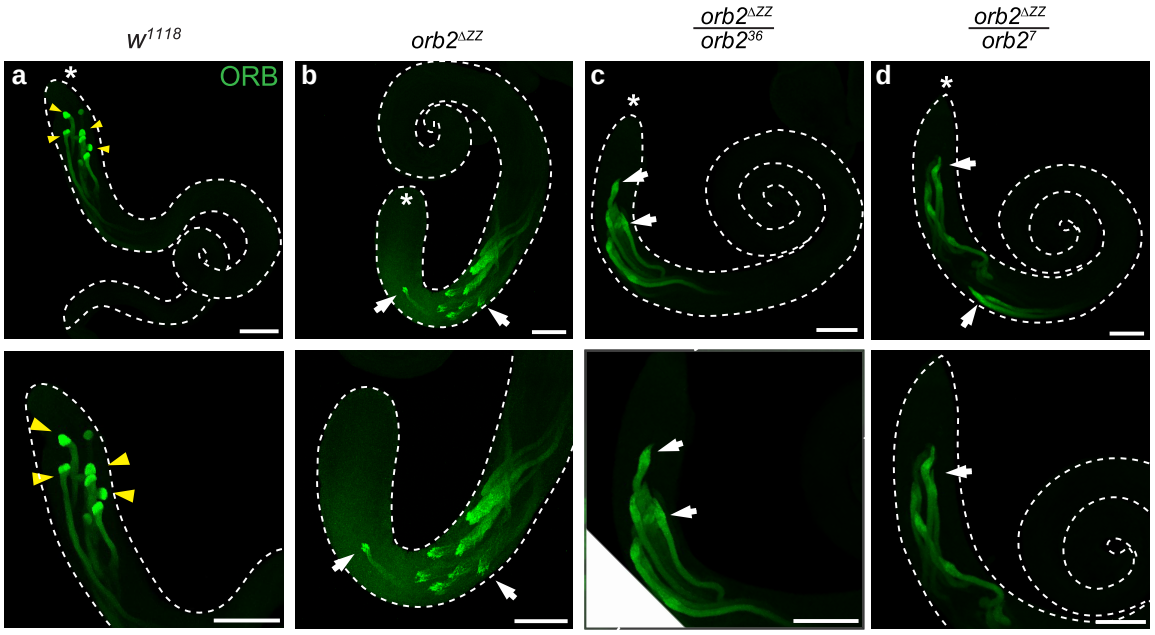

Fig. 7. Spatial distribution of ORB protein is disrupted in $orb2^{\Delta ZZ}$ testes. Laser-scanning confocal micrographs of whole adult testes stained for ORB. a) w^{1118}; b) $orb2^{\Delta ZZ}$; c) $orb2^{\Delta ZZ}/orb2^{36}$; d) $orb2^{\Delta ZZ}/orb2^{7}$. Asterisk (*) indicates the apical tip of the testis; scale bars represent 100 μm; arrowheads in (a) indicate localized ORB protein, concentrated at the distal ends of cysts of elongating spermatids; arrows in (b) to (d) indicate abnormal localization and/or expression patterns in mutant testes. The images shown are representative of 100% of testes examined: w^{1118} ($n = 15$); $orb2^{\Delta ZZ}$ ($n = 12$); $orb2^{\Delta ZZ}/orb2^{36}$ ($n = 13$); $orb2^{\Delta ZZ}/orb2^{7}$ ($n = 10$).

($orb2^{\Delta ZZ}$ $n = 36$, $orb2^{\Delta ZZ}/orb2^{36}$ $n = 24$, $orb2^{\Delta ZZ}/orb2^{7}$ $n = 23$, w^{1118} $n = 43$). Scattering of the actin cones began earlier in $orb2^{\Delta ZZ}$ testes compared to $orb2^{\Delta ZZ}/orb2^{36}$ and $orb2^{\Delta ZZ}/orb2^{7}$ (Fig. 5, b to d panels ii). In all three mutant genotypes, cysts in the late stages of individualization contained extremely scattered actin cones, spanning a large portion of each testis (Fig. 5, b to d, panels iii).

We conclude that individualization fails in $orb2^{\Delta ZZ}$ testes. This failure is likely to be the cause of male sterility that we observed in mutant adult males.

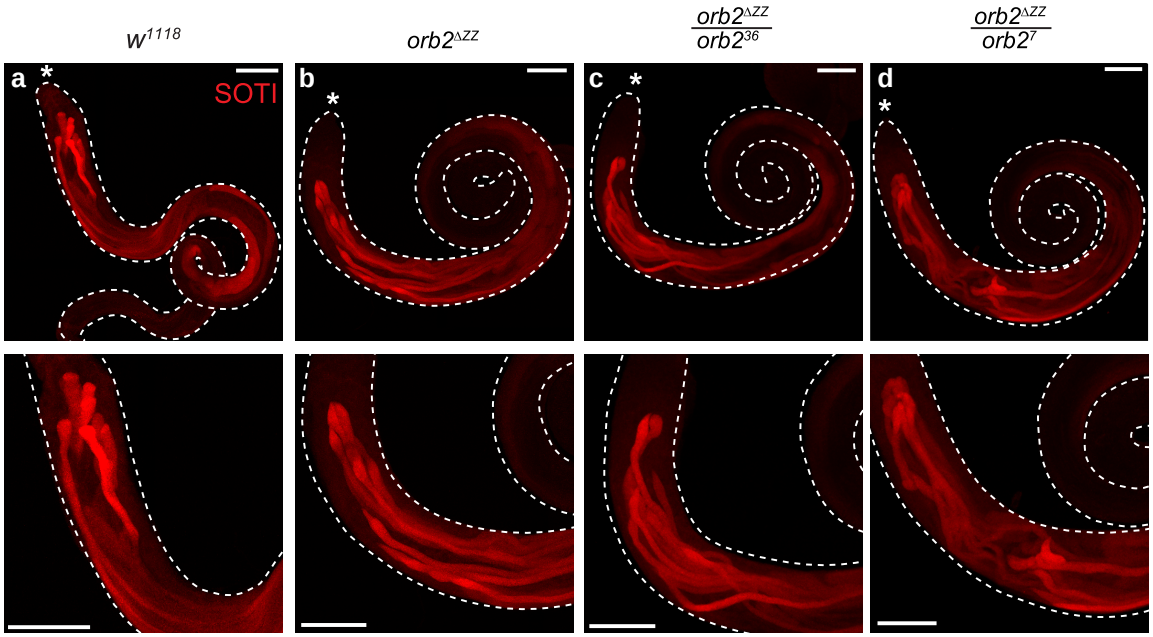

Fig. 8. Spatial distribution of SOTI protein is disrupted in $orb2^{\Delta ZZ}$ testes. Laser-scanning confocal micrographs of whole adult testes stained for SOTI. a) w^{1118}; b) $orb2^{\Delta ZZ}$; c) $orb2^{\Delta ZZ}/orb2^{36}$; d) $orb2^{\Delta ZZ}/orb2^{7}$. Asterisk (*) indicates the apical tip of the testis; scale bars represent 100 μm. The images shown are representative of 100% of testes examined: w^{1118} ($n = 14$); $orb2^{\Delta ZZ}$ ($n = 12$); $orb2^{\Delta ZZ}/orb2^{36}$ ($n = 14$); $orb2^{\Delta ZZ}/orb2^{7}$ ($n = 13$).

The ZZ domain is required for enrichment of IMP, ORB and SOTI proteins at the distal tip of elongating spermatids

In elongating spermatids, proteins such as IMP, ORB, and SOTI are enriched toward the distal end (i.e. opposite end of the spermatid to where the nuclei reside) and SOTI is required for spermatid individualization (Barreau et al. 2008; Fabrizio et al. 2008; Kaplan et al. 2010; Gilmutdinov et al. 2021). We found that deletion of the ZZ domain resulted in weaker enrichment of all three of these proteins at the distal end with the proteins more dispersed along the spermatids (Fig. 6, a to d for IMP, Fig. 7, a to d for ORB and 8a-d for SOTI). Furthermore, loss of the ZZ domain resulted in a "flared paintbrush" appearance of the distal end compared to the rounded and compact shape in wild type. Since the ORB2ΔZZ protein distribution is similar to full-length ORB2 (Fig. 2), these results suggest that deletion of the ZZ domain disrupts the organization and polarization of the distal portion of spermatid cysts leading to delocalization of a subset of IMP, ORB and SOTI proteins.

The cleaved caspase-3 gradient is disrupted in $orb2^{\Delta ZZ}$ mutants

The SOTI protein gradient has been shown to be important for the successful completion of individualization. Specifically, the SOTI gradient regulates an opposing gradient of activated (also called cleaved) caspase-3 (Kaplan et al. 2010). Cleaved caspase-3 (CC3) is localized in a pattern opposite to that of SOTI protein because SOTI represses Caspase-3 via a Cullin-based E3 ubiquitin ligase complex. In wild-type cysts, low levels of CC3 are at the distal end of the spermatid cyst (Fig. 9a) and activity increases toward the spermatid nuclei, with CC3 concentrated at the IC. This concentration of CC3 activity is pushed down the length of the cyst along with cystic bulge by the IC as it travels away from the nuclei, eventually being discarded inside the waste bag.

Since the SOTI gradient is disrupted in the testes of $orb2^{\Delta ZZ}$ mutants, we asked whether the CC3 gradient was also affected. We found that the CC3 gradient was altered such that CC3 protein was distributed along the length of the cyst (Fig. 9, b and c). In addition, we found that the cystic bulges in $orb2^{\Delta ZZ}$ testes were wider and longer compared to wild-type testes, and waste bags were completely absent.

Together, our data are consistent with a model in which the ZZ domain is required for organization of the distal region of the spermatid cyst and establishment of the SOTI gradient, which in turn regulates CC3 production and successful spermatid individualization.

Discussion

Here, we have shown that the ZZ domain of ORB2 is required for male fertility and is involved in at least two aspects of spermatogenesis: meiosis of spermatocytes to produce spermatids and, subsequently, spermatid individualization to produce mature sperm. We observed defects in meiosis in $orb2^{\Delta ZZ}$ mutants, both when homozygous and when present in one copy when hemizygous with an *orb2* deletion. While these meiotic defects were of low penetrance, it is important to note that many, small nuclei could lead to the formation of numerous small actin cones (multiple cones per spermatid, i.e. many more than 64 cones per cyst) with subsequent failure of individualization and consequent male sterility.

The phenotypes of $orb2^{\Delta ZZ}$ mutants show both similarities to and differences from those of the *orb2* null mutants, as well as $orb2^{\Delta Q}$ and $orb2^{R}$ mutants, which respectively, delete the polyQ domain or the 3′UTR. First, while the *orb2* null mutant and $orb2^{\Delta ZZ}$ mutant are both completely male sterile, the $orb2^{R}$ mutant shows incomplete sterility (Gilmutdinov et al. 2021). Second, $orb2^{\Delta ZZ}$ mutants show an increase in transcript and protein levels. This contrasts with $orb2^{R}$, for which a reduction of transcript and protein expression has been observed, and the $orb2^{\Delta Q}$ allele, whose transcript and protein expression is comparable to wild type (Keleman et al. 2007; Gilmutdinov et al. 2021). Third, $orb2^{\Delta ZZ}$ mutants largely complete meiosis (albeit with defects in Nebenkern

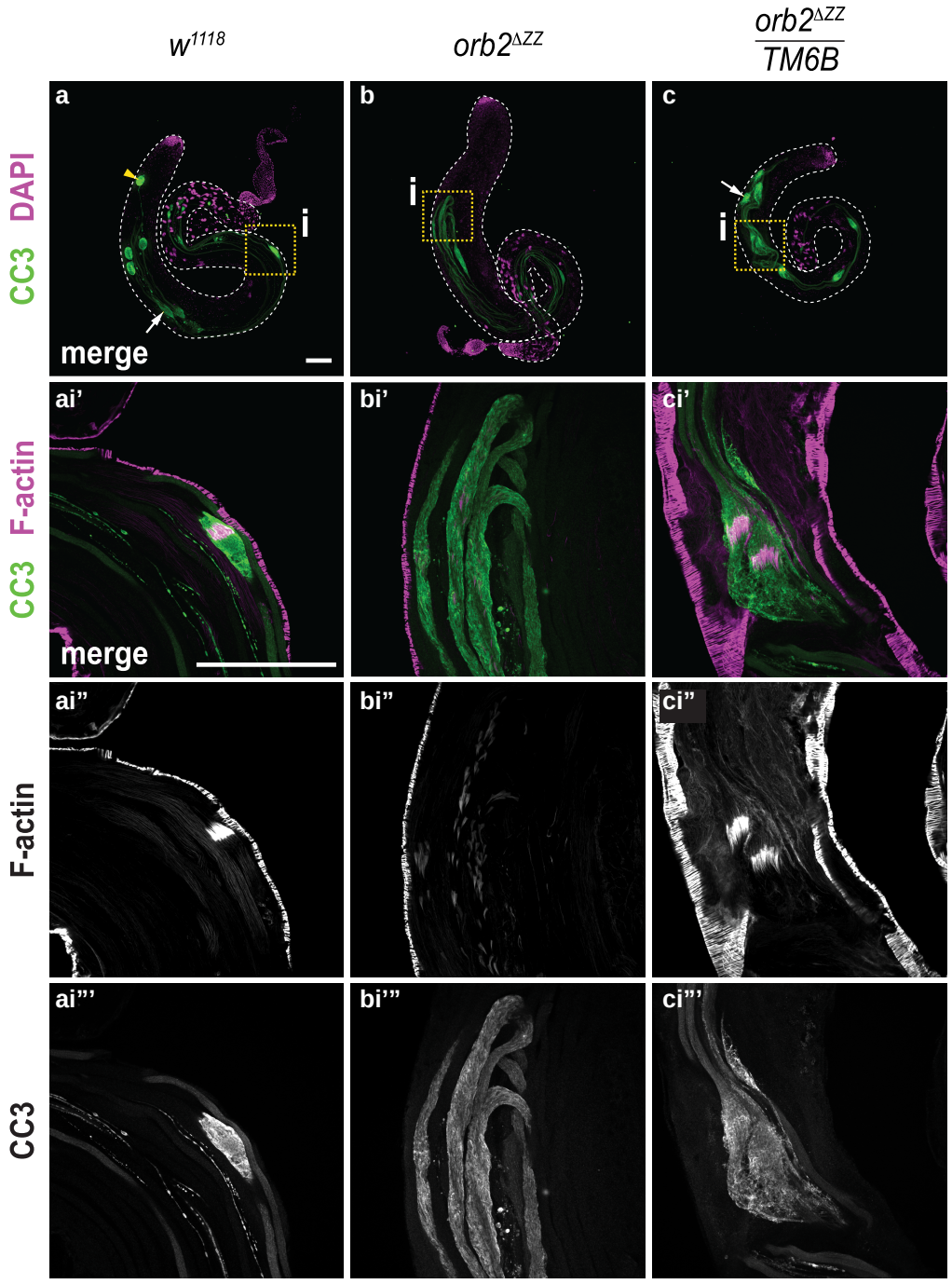

Fig. 9. The cleaved caspase-3 (CC3) protein gradient is disrupted in $orb2^{\Delta ZZ}$ testes. Laser-scanning confocal micrographs of whole adult testes stained in (a)-(c) for CC3 (green) and DNA (DAPI, magenta) or (a')-(c"') for CC3 (green) and F-actin (rhodamine phalloidin, magenta). a) w^{1118}; b) $orb2^{\Delta ZZ}$; c) $orb2^{\Delta ZZ}$/*TM6B*. Arrows indicate examples of cystic bulges; arrowhead indicates example of a waste bag. Scale bar represents 100 μm. Micrographs are representative of 100% of testes examined in three experiments: w^{1118} $n \geq 11$, $orb2^{\Delta ZZ}$/*TM6B* $n \geq 10$, $orb2^{\Delta ZZ}$ $n \geq 16$.

formation that are statistically significant but of low penetrance) whereas *orb2* null mutants largely fail to complete meiosis and meiotic defects have not been observed in $orb2^{R}$ mutants (Xu et al. 2012; Gilmutdinov et al. 2021). Fourth, in *orb2* null mutants, the IC is never assembled and individualization never takes place, whereas $orb2^{\Delta Q}$, $orb2^{R}$, and our $orb2^{\Delta ZZ}$ mutants all show disordered/scattered ICs (Keleman et al. 2007; Xu et al. 2012; Gilmutdinov et al. 2021). However, in contrast to $orb2^{\Delta Q}$ and $orb2^{R}$ alleles, which have a penetrance of ~40% and ~80% respectively (Xu et al. 2012, 2014; Gilmutdinov et al. 2021), the scattered IC phenotype is 100% penetrant in $orb2^{\Delta ZZ}$ mutants. In summary, while there are similarities between the $orb2^{\Delta ZZ}$ allele and other *orb2* alleles, the $orb2^{\Delta ZZ}$ allele does not fully phenocopy any other *orb2* alleles; rather, the $orb2^{\Delta ZZ}$ allele shows a distinct level of RNA and protein expression, and its developmental phenotype is more severe than both previously reported partial gene deletions. Future studies will focus on elucidating the mechanistic bases for these phenotypic differences.

The observation that the polyQ domain is required for sperm individualization suggests that the ability of ORB2A and ORB2B

to oligomerize is required for the completion of spermatogenesis (Xu et al. 2012). The polyQ domain has been associated with translational activation of ORB2 bound transcripts (White-Grindley et al. 2014; Khan et al. 2015). Our recent analysis of the role of the ZZ domain in the early embryo has shown that it is required for negative regulation of ORB2's target mRNAs (Low et al. 2025); however, since ORB2B is the only isoform expressed in early embryos, that study does not shed light on the possible role of the ZZ domain in translational activation in the context of ORB2A-ORB2B hetero-oligomers. The fact that, as described above, *orb2*$^{\Delta ZZ}$ mutants share several phenotypes with *orb2*$^{\Delta Q}$ mutants is consistent with a role for the ZZ domain in ORB2-mediated translational activation.

We have recently shown that the ZZ domain interacts with all of the components of the 43S translation preinitiation complex (PIC) in early embryos (Low et al. 2025). During cap-dependent translation initiation, the PIC is recruited to the 5′-end of an mRNA by eIF4F, which includes eIF4A, the cap-binding protein eIF4E, and eIF4G. If ORB2's interaction with the PIC is conserved in testes, we speculate that translational activation by the ORB2A-ORB2B heteromers may be mediated at least in part by recruitment of the 43S PIC to target mRNAs. We recently reported a link between ORB2 and the testis-specific eIF4E paralog, eIF4E5, which is consistent with such a role (Shao et al. 2023): ORB2 and eIF4E5 genetically interact to control spermatid cyst polarization; additionally, eIF4E5 mutants display defects in SOTI protein accumulation and defective individualization, resulting in male sterility. Notably, the *soti* and *orb* mRNAs have been identified as direct targets of ORB2 (Xu et al. 2012) and we have shown that deletion of the ZZ domain does not affect RNA-binding by ORB2 (Low et al. 2025). Thus, a plausible hypothesis is that misregulation of these mRNAs is at least in part the cause of the spermatogenesis defects in *orb2*$^{\Delta ZZ}$ mutants. Whether PIC and eIF4E5 interaction is the basis for ORB2-mediated activation in the testis and the functional role of ORB2's ZZ domain in regulation of the *soti* and *orb* mRNAs will be interesting areas for future study.

Data availability

The authors affirm that all of the data necessary for confirming the conclusions of the article are present within the article, figures, and Supplementary Fig. 1.

Supplemental material available at G3 online.

Acknowledgments

We thank Eli Arama and Paul Macdonald for providing anti-SOTI and anti-IMP antibodies, respectively; and Kimberly Lau and Paul Paroutis of the SickKids Imaging facility for assistance with imaging. We used the resources provided by FlyBase. Stocks were obtained from the Bloomington Drosophila Stock Center (NIH P0OD018537). The anti-ORB2 4G8 and anti-ORB 6H4 antibodies listed in Materials and Methods were obtained from the Developmental Studies Hybridoma Bank, created by the NICHD of the NIH and maintained at The University of Iowa, Department of Biology, Iowa City, IA 52242.

Funding

This research was supported by grants from the Canadian Institutes of Health Research PJT-159702 (HDL), PJT-190124 (HDL) and the Natural Sciences and Engineering Research Council of Canada (NSERC) RGPIN-2022-05163 (JAB). TCHL was supported in part by a Natural Sciences and Engineering Council of Canada (NSERC) Alexander Graham Bell Canada Graduate Scholarship - Master's (CGS-M) 496345-2016 and a University of Toronto Open Fellowship; BLF was supported in part by a Department of Molecular Genetics Eric Hani Fellowship, University of Toronto, a University of Toronto Open Fellowship, and a Natural Sciences and Engineering Research Council of Canada (NSERC) Post-Graduate Scholarship (PGS-D) #588703-2024).

Conflicts of interest

The authors declare that they have no conflicts of interest.

Literature cited

Barreau C, Benson E, Gudmannsdottir E, Newton F, White-Cooper H. 2008. Post-meiotic transcription in Drosophila testes. Development. 135:1897–1902. https://doi.org/10.1242/dev.021949.

Danielsen JR *et al.* 2012. DNA damage-inducible SUMOylation of HERC2 promotes RNF8 binding via a novel SUMO-binding Zinc finger. J Cell Biol. 197:179–187. https://doi.org/10.1083/jcb.201106152.

Diehl C *et al.* 2016. Structural analysis of a Complex between small ubiquitin-like modifier 1 (SUMO1) and the ZZ domain of CREB-binding protein (CBP/p300) reveals a new interaction surface on SUMO. J Biol Chem. 291:12658–12672. https://doi.org/10.1074/jbc.M115.711325.

Fabrizio JJ *et al.* 2008. Imp (IGF-II mRNA-binding protein) is expressed during spermatogenesis in Drosophila melanogaster. Fly (Austin). 2:47–52. https://doi.org/10.4161/fly.5659.

Gilmutdinov R *et al.* 2021. The 3′UTR of the Drosophila CPEB translation factor gene orb2 plays a crucial role in spermatogenesis. Development. 148:dev198788. https://doi.org/10.1242/dev.198788.

Hake LE, Richter JD. 1994. CPEB is a specificity factor that mediates cytoplasmic polyadenylation during Xenopus oocyte maturation. Cell. 79:617–627. https://doi.org/10.1016/0092-8674(94)90547-9.

Ivshina M, Lasko P, Richter JD. 2014. Cytoplasmic polyadenylation element binding proteins in development, health, and disease. Annu Rev Cell Dev Biol. 30:393–415. https://doi.org/10.1146/annurev-cellbio-101011-155831.

Kaplan Y, Gibbs-Bar L, Kalifa Y, Feinstein-Rotkopf Y, Arama E. 2010. Gradients of a ubiquitin E3 ligase inhibitor and a caspase inhibitor determine differentiation or death in spermatids. Dev Cell. 19:160–173. https://doi.org/10.1016/j.devcel.2010.06.009.

Keleman K, Krüttner S, Alenius M, Dickson BJ. 2007. Function of the Drosophila CPEB protein Orb2 in long-term courtship memory. Nat Neurosci. 10:1587–1593. https://doi.org/10.1038/nn1996.

Khan MR *et al.* 2015. Amyloidogenic oligomerization transforms Drosophila Orb2 from a translation repressor to an activator. Cell. 163:1468–1483. https://doi.org/10.1016/j.cell.2015.11.020.

Legge GB *et al.* 2004. ZZ domain of CBP: an unusual zinc finger fold in a protein interaction module. J Mol Biol. 343:1081–1093. https://doi.org/10.1016/j.jmb.2004.08.087.

Li H *et al.* 2022. Fly cell atlas: a single-nucleus transcriptomic atlas of the adult fruit fly. Science. 375:eabk2432. https://doi.org/10.1126/science.abk2432.

Liu J *et al.* 2020. Structural insight into binding of the ZZ domain of HERC2 to histone H3 and SUMO1. Structure. 28:1225–1230 e3. https://doi.org/10.1016/j.str.2020.07.003.

Low TCH, *et al.* 2025. The ORB2 RNA-binding protein negatively regulates its target transcripts during the Drosophila maternal-to-zygotic transition via its functionally conserved Zinc-binding 'ZZ' domain. Genetics. iyaf241. https://doi.org/10.1093/genetics/iyaf241.

Mastushita-Sakai T, White-Grindley E, Samuelson J, Seidel C, Si K. 2010. Drosophila Orb2 targets genes involved in neuronal growth, synapse formation, and protein turnover. Proc Natl Acad Sci U S A. 107:11987–11992. https://doi.org/10.1073/pnas.1004433107.

Merkel DJ *et al.* 2013. The C-terminal region of cytoplasmic polyadenylation element binding protein is a ZZ domain with potential for protein-protein interactions. J Mol Biol. 425:2015–2026. https://doi.org/10.1016/j.jmb.2013.03.009.

Ozturk-Colak A *et al.* 2024. FlyBase: updates to the Drosophila genes and genomes database. Genetics. 227:iyad211. https://doi.org/10.1093/genetics/iyad211.

Park S *et al.* 2017. Role of the CBP catalytic core in intramolecular SUMOylation and control of histone H3 acetylation. Proc Natl Acad Sci U S A. 114:E5335–E5342. https://doi.org/10.1073/pnas.1703105114.

Ponting CP, Blake DJ, Davies KE, Kendrick-Jones J, Winder SJ. 1996. ZZ and TAZ: new putative zinc fingers in dystrophin and other proteins. Trends Biochem Sci. 21:11–13. https://doi.org/10.1016/S0968-0004(06)80020-4.

Shao L *et al.* 2023. Eukaryotic translation initiation factor eIF4E-5 is required for spermiogenesis in Drosophila melanogaster. Development. 150:dev200477. https://doi.org/10.1242/dev.200477.

Stepien BK *et al.* 2016. RNA-binding profiles of Drosophila CPEB proteins Orb and Orb2. Proc Natl Acad Sci U S A. 113:E7030–E7038. https://doi.org/10.1073/pnas.1603715113.

Tencer AH *et al.* 2022. The ZZ domain of HERC2 is a receptor of arginylated substrates. Sci Rep. 12:6063. https://doi.org/10.1038/s41598-022-10119-w.

Vedelek V *et al.* 2018. Analysis of Drosophila melanogaster testis transcriptome. BMC Genomics. 19:697. https://doi.org/10.1186/s12864-018-5085-z.

Wang YY *et al.* 2021. Molecular and structural mechanisms of ZZ domain-mediated cargo selection by Nbr1. EMBO J. 40:e107497. https://doi.org/10.15252/embj.2020107497.

White-Grindley E *et al.* 2014. Contribution of Orb2A stability in regulated amyloid-like oligomerization of Drosophila Orb2. PLoS Biol. 12:e1001786. https://doi.org/10.1371/journal.pbio.1001786.

Xu S, Hafer N, Agunwamba B, Schedl P. 2012. The CPEB protein Orb2 has multiple functions during spermatogenesis in Drosophila melanogaster. PLoS Genet. 8:e1003079. https://doi.org/10.1371/journal.pgen.1003079.

Xu S, Tyagi S, Schedl P. 2014. Spermatid cyst polarization in Drosophila depends upon apkc and the CPEB family translational regulator orb2. PLoS Genet. 10:e1004380. https://doi.org/10.1371/journal.pgen.1004380.

Editor: H. Salz